Towards Exceptional Icephobicity with Chionophile-inspired Durable Biomimetic Coatings

Halar Memon[a], Davide S.A. De Focatiis[a], Kwing-So Choi[a], and Xianghui Hou[a]*

[a]Faculty of Engineering, University of Nottingham, University Park, Nottingham NG7 2RD, UK;

*Correspondence: xianghui.hou@nottingham.ac.uk.

Abstract

Liquid-infused polymeric surfaces have demonstrated promising icephobicity. However, the capability to maintain the icephobic performance after material damage has been a challenge, both in terms of conserving a smoother surface and the replenishment of infused liquid. Cetacean skin possesses a microscopically smooth texture in the form of cells lubricated with lipid proteins and consists of structural fibres that ensure durability. Concerning the structure of cetacean skin, glycerol infused fibre-reinforced polyurethane coatings (GIFRP) were proposed. Instead of hosting the lipid proteins, the coatings were infused with glycerol, a known cryoprotectant to induce the supercooling of water, a strategy inspired by wood frogs and red flat dark beetles to prevent freezing. The inclusion of glycerol delayed water droplet freezing duration by 659%, while negligible frost accumulated on the fabricated coatings during anti-icing tests. The reinforcement of fibres was effective and the surface damage was reduced by a factor of 4, compared to the pure polyurethane coatings under erosion impact. The incorporation of fibres has proven to be beneficial for infused-liquid replenishment and the slow-releasing capabilities of GIFRP coatings. Minimised surface deterioration and the continued presence of glycerol on GIFRP coatings demonstrated a small increase in ice adhesion from 0.22 kPa to 0.77 kPa after the erosion tests, one of the lowest values reported in the literature after substantial surface damage. The concept inspired by cetacean skin and the cryoprotective features of chionophiles was instrumental in keeping the ice adhesion under 1 kPa after erosion impact.

Keywords: bio-mimicry; freezing delay; ice adhesion; durability; icephobic

1 Introduction

Frost formation has been a costly inconvenience to engineering applications and considerable energy resources are required to de-ice, making many applications complicated and inefficient. Over the last few decades, passive de-icing has been a growing research topic and it has been suggested that inspiration could come from nature to develop a bio-inspired design to mitigate/resist ice formation (anti-icing) and/or to remove the formed ice easily (de-icing). Several bionic ideas inspired by mussels[1] and skin[2] were put to test to aid icephobicity and promising results were reported. Biomimetic designs were also inspired by fish proteins, such as the use of anti-freezing proteins (AFPs) to reduce the supercooling point and delay the ice nucleation process over the surfaces. Two typical approaches were used: directly grafting AFPs on functionalized surfaces[3-4] and mimicking the ice depressing effect of AFPs using a direct infusion of cryoprotectants on low-surface energy functionalized surfaces[5-6]. The direct role of AFPs on ice nucleation or ice adhesion is questionable as hydrophobicity-induced icephobicity[7-9] and solid/liquid interfaces[3-4] play an influential part.

Apart from bio-inspired concepts, slippery liquid-infused coatings/surfaces have gained significant popularity among the research community[10-12]. The fabrication of slippery surfaces can be achieved by either a physical infusion of liquids in the polymeric matrix or by impregnating the surface asperities. In both cases, the infused liquid works by either delaying the ice formation or by forming more loosely bonded ice on the surface. The formation of loosely anchored ice on the surface could be attributed to the reduction in the number of available surface cavities since these are levelled due to liquid impregnation; this may hinder the anchoring of ice in the surface asperities. Furthermore, the use of a smoother morphology has been advised in the literature to create low ice adhesion surfaces[13-14].

The use of AFPs-inspired coatings or liquid infused coatings poses performance challenges such as coating durability and liquid retention within a material matrix. For example, several studies indicated the depletion of infused liquid after several cyclic de-icing tests or during mechanical durability tests[15-18]. Thus, there is a need for an effective material system or mechanism that could work to provide the necessary durability, help with liquid replenishment, and maintain a soft and smooth surface to induce interfacial cavitation/anchor-free ice[18-19].

In nature, cetacean skin is characterised by a number of microscopic qualities such as smoothness, the lack of hair follicles, and lipid-infused surfaces, which emits oil to improve hydrodynamics. On top of these qualities, the skin consists of keratins, collagen and elastin fibres that work to provide mechanical strength and elasticity to the skin. These fibres make the skin more adaptable to repetitive loads (without undergoing a plastic deformation). The concept of fibre reinforcement, mimicking collagen fibres, could also be used for icephobic surfaces to improve their structural and mechanical response. Furthermore, a microscopically smooth surface could be beneficial for anchor-free ice nucleation and if a weaker or reduced number of ice anchors do occur, then the softer or flexible material could induce interfacial cavitation to pave the easy path for ice to release[18-19]. The concept of lipid droplets, hosted in cetacean skin, can be further mimicked, such as the infusion of a liquid in the flexible material matrix and the selection of liquid can be specifically made to reduce the supercooling point, like chionophiles which emit a cryoprotectant to depress the ice nucleation. Hence, the idea of combining an infused ice-depressing liquid in a reinforced polymer composite could significantly weaken or even inhibit the ice/solid interfaces, whereas the reinforcements could provide necessary durability to maintain the icephobic performance.

In this study, our proposed design concept is inspired by the anatomy of cetacean skin and the coatings mimicked the structure of the skin. A polyurethane (PU) matrix was used to produce a smooth and soft surface, with the matrix infused by a cryoprotectant, glycerol, to reduce the supercooling point and provide a flexible surface. Carbon fibres were incorporated, along with the infused liquid, to provide strength and mimicking collagen fibres in the skin. The icephobic performance of formulated glycerol-infused fibre-reinforced polyurethane (GIFRP) icephobic coatings was evaluated using established de-icing and custom-built anti-icing tests, and the tests were repeated after silicon carbide-based water suspension erosion and overnight water immersion, respectively, to determine the longevity of the coatings.

2 Design of chionopile-inspired cetacean-skin mimicked icephobic coatings

Cetacean skin is an elastic material[20] and consists of three layers: the epidermis (top exposed layer), dermis (intermediate thick layer), and endodermis (blubber)[21]. However, the typical distinction between dermis and epidermis is not as noticeable in cetacean skin. The typical anatomy of cetacean skin is shown in figure 1a. All three layers of the skin consist primarily of collagen and elastin fibres surrounded by the keratins scleroproteins[22]. Most of the skin mechanical structure, strength, and stiffness comes from collagen fibres and keratins, and the elastin fibres, as the name suggests, provide elasticity and extensibility to the skin[20]. Keratins are insoluble, chemically unreactive fibrous macromolecules and they create very tough disulfide cross-linkages across the epidermis[22]. The proposed GIFRP coatings involve two different types of biomimicry: one aspect to mimic cetacean skin and another to mimic chionophiles.

In the proposed coating design, carbon fibres were incorporated in the PU matrix to resemble collagen fibres interwoven in elastin fibres and keratins. In cetacean skin, elastin fibres and keratins are typically interwoven or arranged in a branching pattern in a collagen fibre matrix as

shown in figure 1a, to prevent tearing and limit dispensability. The elastomeric matrix is interlinked by stretchable chains (resembling elastin fibres), which could provide the necessary elasticity, and are connected by strong chemical bonds (for example, vulcanization)[23]. The collagen fibres have high tensile strength (500-1000 kg/cm^2, higher than steel)[24] and the carbon fibres also possess high tensile strength values (35140-35560 kg/cm^2). In other words, the skin is a composite where strong collagen fibres are embedded in a tough elastic elastin fibre matrix, providing the necessary structural strength. Collagen breaks into small segments under load and the fibres disperse the energy along the length of the fibre and prevent the stress from concentrating in one area or transmitting to another fibre segment[23]. Interestingly, fibre-reinforced polymeric coatings also exhibit similar behaviour under load, dispersing the energy along the fibre length and fibre breakage under the erosion impacts[25]. The impacts on the polymeric matrix result in chipping and fracture of fibres instead of material fractures, thus, the composite ability to withstand repetitive impact loads is greatly enhanced.

The top exposed layer of cetacean skin epidermis provides an elastic and relatively smooth surface. This kind of skin completely lacks hair follicles which would otherwise increase drag in the water. Another important epidermal relationship for cetacea lies in the variable elasticity of the skin itself which could be attributed to the high ratio of elastin fibres in the dermis[22]. Smoother surface or lower elastic modulus in elastomeric coatings could be utilized for easy release of ice[18-19], whereas the lack of surface anomalies, like the absence of hair follicles in cetacean skin, means that ice is hard to anchor or discouraged towards heterogeneous ice nucleation.

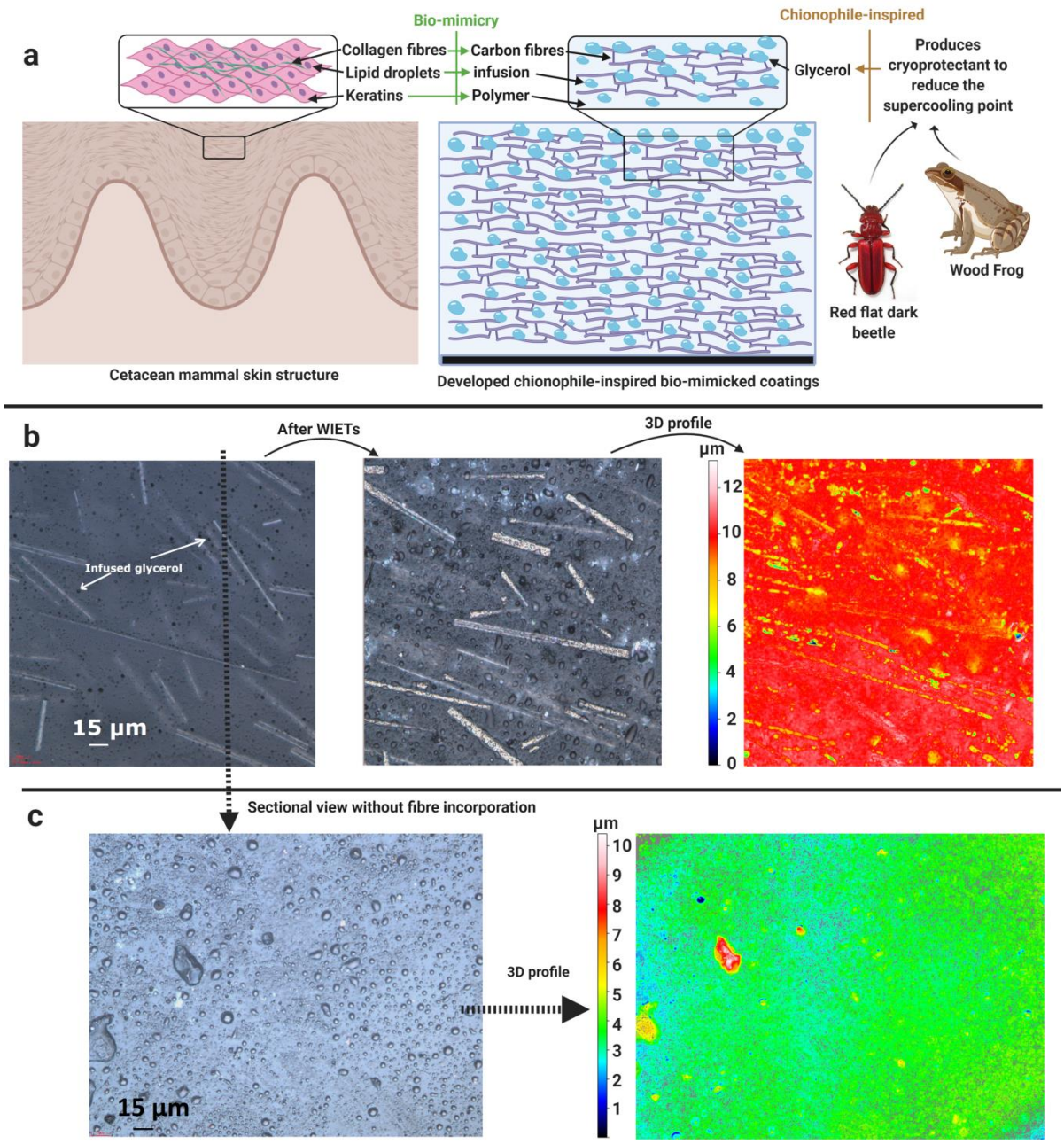

Figure 1: The microstructural design of the developed coatings, mimicked by the anatomy of a cetacean mammal skin and inspired by the cryoprotective properties of wood frog and red flat dark beetles (a), the microstructural images of GIFRP coatings and the same coating after the erosion tests, including a 3D picture (b), and the sectional view of PU-20gly coatings (after it is cut) and their 3D profile (c) (created using Biorender.com)

Interestingly, the cetacean skin structure also hosts phospholipid-rich cornified layers in the form of lipid droplets[26]. The presence of these lipid droplets in cetacean skin improves hydrodynamics by continually exuding oil droplets which help to lubricate the skin allowing the water to pass more smoothly. Similar to the diffusion of oil droplets in cetacean skin, the proposed GIFRP coating will host a number of glycerol droplets as shown in figure 1a and these droplets could be slowly diffused on the surface to impart and maintain icephobicity. Glycerol is categorized as a cryoprotectant and is known to repress the freezing point of water and enhance supercooling[27]. Thus, the presence of glycerol on the surface may weaken the ice/surface interfaces, which could reduce ice adhesion strength. The inclusion of glycerol is inspired by chionophiles such as the wood frog and red flat dark beetles that use polyhydric alcohols to prevent extracellular ice formations by a colligative action of cryoprotectants and regulate the freeze concentration of cells from reaching an injurious level[28]. For example, the beetles produce antifreeze glycolipids and proteins and lower the supercooling point. They go into diapause and inhibit the ice nucleation by producing multimolar concentration glycerol that protects them from freezing[29]. The presence of glycerol on the proposed surface is intended to repress the ice nucleation as glycerol forms stronger hydrogen bonds with water molecules and works to disrupt the ice crystal lattice formation by competing with water-to-water hydrogen bonding unless the temperature is significantly lowered[30]. However, hosting glycerol droplets may result in some degree of coating dissolution over time and the supercooling effect induced by glycerol relies on effectual miscibility with water[31]. Thus, uniform distribution and continued replenishment of glycerol are necessary to repress the ice nucleation. The presence of glycerol to impart

icephobicity is ensured by a uniform distribution of glycerol pockets in the coating matrix and slow diffusion of glycerol on the surface.

To summarize, carbon fibres were incorporated in a PU matrix to mimic cetacean skin anatomy and the infusion of glycerol was inspired by chionophiles as illustrated in figure 1a. The fibre-reinforced polymers impart overall durability and the infusion of glycerol is intended to create supercooling conditions that may inhibit/resist ice nucleation and may work to form weaker ice/solid interfaces.

3 Results and discussion

The coatings discussed in this section are pure PU, 20 wt% infusion of glycerol in PU matrix (PU-20gly), 20 wt% incorporation of carbon fibres in PU matrix (PU-20CF), and 20 wt% infusion of glycerol and 20 wt% incorporation of carbon fibres in PU matrix (GIFRP) coatings.

3.1 Microstructure and Shore hardness analysis

The surface roughness (R_a) on pure PU coating was measured at 0.08 ± 0.01 µm. The inclusion of glycerol generated liquid pockets in the polyurethane matrix and the surface roughness changed to 3.20 ± 0.07 µm. The surface roughness excluding the glycerol pockets was measured at 0.14 ± 0.05 µm and including glycerol pockets at 3.20 ± 0.07 µm. To understand the uniformity of the glycerol pockets in PU-20gly coatings, free-standing layers of similar thickness (4 mm) were fabricated. These layers were then bifurcated using a sharp blade and the glycerol infusion through the coating thickness was observed via a scanning electron microscope (SEM) system. The sectional view of PU-20gly coatings is shown in figure 1c. The figure clearly indicates that the glycerol was uniformly distributed and the coating capability to retain the liquid inside the polyurethane matrix.

Figure 1b illustrates the microstructural image of GIFRP coatings. The observation of figure 1b indicates that the uniformity of carbon fibres throughout the polymeric matrix and the glycerol pockets are in sizes of 0.1 ~ 2 μm. The sectional uniformity of glycerol pockets distribution observed on PU-20gly coatings could be assumed for GIFRP coatings as there was no disparity in coating application methods. The surface roughness (R_a) of 0.12 ± 0.03 μm was measured on PU-CF20 coatings and 0.22 ± 0.04 μm on GIFRP coatings. As-received aluminium substrates (Al2024) were also used for a comparative purpose and the microstructural image of the aluminium is shown in figure S1. The surface roughness (R_a) of 0.90 ± 0.01 μm was measured on the aluminium substrates, a higher magnitude of surface roughness as compared to all the polymeric samples used in this study. The microstructural images of other polymeric coatings are shown in figure S2. Shore hardness measurement conducted on the coatings showed that the hardness on pure PU coatings decreased from 40D to 33D after the inclusion of glycerol, whereas on fibre-reinforced coatings, it decreased from 65D to 54D. Thus, the hardness of the coatings decreased with the liquid infusion and the hardness values obtained on the fibre-reinforced coatings are higher than those of pure PU or PU-20gly coatings.

3.2 Surface analysis after erosion

The surface morphology of the developed coatings is shown in figure 1 and can be explained in two distinctive properties: change in surface roughness and glycerol retention after erosion tests. The erosion test setup is described in the experimental section. Firstly, the surface roughness (R_a) on pure PU coatings changed from 0.08 ± 0.01 μm to 0.45 ± 0.05 μm after WIETs and from 0.14 ± 0.05 μm to 0.70 ± 0.10 μm on PU-20gly coatings. As compared to pure PU coatings, the change in surface roughness (R_a) after erosion attack was greatly reduced on fibre-reinforced coatings, indicating the incorporation of fibres mitigated the erosion impact. The microstructural

image of GIFRP coatings and the same coating after the erosion tests are shown in figure 1b. The surface roughness of PU-20CF coatings changed from 0.12 ± 0.03 μm to 0.15 ± 0.02 μm after WIETs. Whereas on bio-inspired GIFRP coatings, surface roughness increased from 0.22 ± 0.04 μm to 0.32 ± 0.04 μm after WIETs. It is imperative to mention that the infused liquid seems to have been retained on GIFRP coatings after the erosion tests, observed in figure 1b. The coatings could have either exposed the infused glycerol after the erosion or furnished it via a slow-releasing mechanism.

3.3 Icephobic performance of the GIFRP coatings

3.3.1 Evaluation of static anti-icing properties

Static water droplet icing delay was measured on all the studied polymeric coatings including on the aluminium substrates and the results are summarised in figure 2a. Distilled water droplets froze in ~7 seconds on the aluminium substrates, whereas the droplets took 44~49 seconds to freeze on pure PU and PU-20CF coatings. The freezing time was significantly delayed on PU-20gly and GIFRP coatings to ~364-372 seconds and the inclusion of glycerol resulted in a ~659% increase in water droplet icing delays as compared to that of pure PU coatings. The incorporation of fibres enhanced the water droplet freezing delay time by ~11% in the case of pure PU coatings and ~2% in the case of the glycerol infused PU coatings.

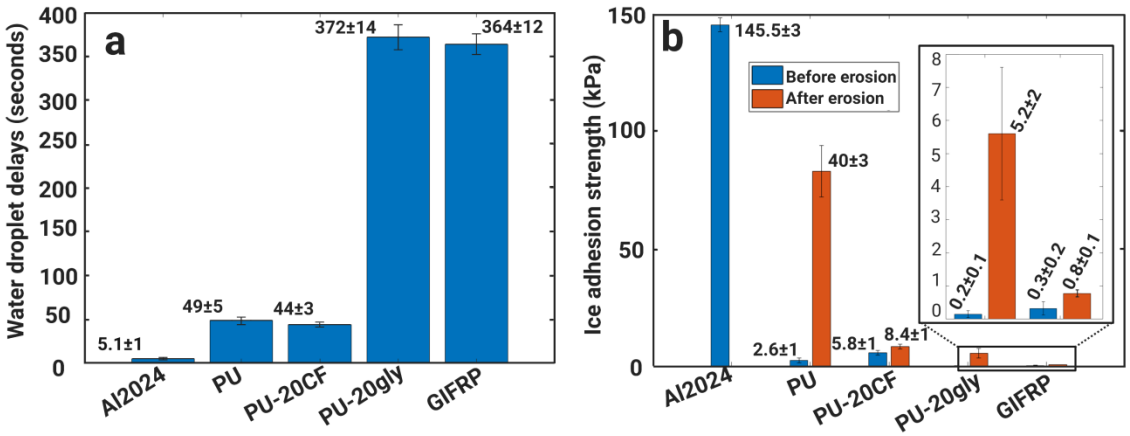

Figure 2: Water droplet icing delay (a) and de-icing results before and after the erosion tests (b) on developed and the aluminium samples

Static frost accumulation tests were also conducted on the studied samples with and without the inclusion of glycerol. The test duration was one hour for both the static and dynamic frost accumulation tests and the nebulised water aerosols were maintained throughout the tests and the volume of nebulised water was monitored. In comparison to the aluminium substrates, PU and PU-20CF coatings demonstrated a lower frost accumulation. Both polymeric coatings accumulated ~35-36 mg of frost as compared to 76 mg on the aluminium substrates. The glycerol infused coatings weighed heavier after the anti-icing tests as compared to the dry PU coatings and resulted in a similar weight as the aluminium substrates. Visual inspection of GIFRP coatings in figure 3a suggests that the frost accumulation was more like condensate accumulation and the coatings accumulated negligible frost during the test duration. The increased mass could be justified due to the hydrophilic nature of the infused PU coatings as compared to that of the dry PU coatings and the hygroscopic nature of glycerol, which collected the condensed water, mainly during the frost accumulation tests. Figure 3a also shows accumulated frost on the exposed metal side, signifying the ice depressing role of the fabricated coatings. The glycerol infused polyurethane coatings demonstrated promising anti-icing

performance in the static anti-icing tests and the coatings were successful in resisting the frost accumulation/ice nucleation on the coating surface.

3.3.2 Dynamic frost formation

Dynamic anti-icing tests were performed via a custom-made rotatable apparatus at the rotational speeds of 30 rpm and 300 rpm. The speeds of the rotatable sample holder were selected to simulate near-static and dynamic conditions and to minimise the effect of enhanced air circulation on frost accumulation. The major difference between the static and dynamic anti-icing tests was the relative movement of samples. In the static test, the samples were placed stationary; whereas in the dynamic test, the samples were mounted on a rotatable sample holder. The results of dynamic frost accumulation tests on the metallic substrates and substrates with PU coatings are summarized in figure 3b. On average, the dynamic anti-icing tests generated ~565% more frost at 300 rpm as compared to the tests conducted at 30 rpm. The enhanced frost accumulation could be due to higher air circulation in the chamber as the rotation may influence the airflow and result in higher accumulations. The frost accumulation did not change significantly on the surfaces at 30 rpm, however, correlated with the results obtained at 300 rpm as shown in figure 3c. At 300 rpm speed, a similar magnitude of frost formation of ~210 mg and ~219 mg were observed on PU and PU-20CF coatings, respectively. The metallic substrates accumulated ~301 mg of frost at a similar speed. Once again, the glycerol-infused polyurethane coatings were significantly heavier as compared to that of pure PU coatings and ~293 mg and ~374 mg of frost/condensate were accumulated on PU-20gly and GIFRP coatings, respectively.

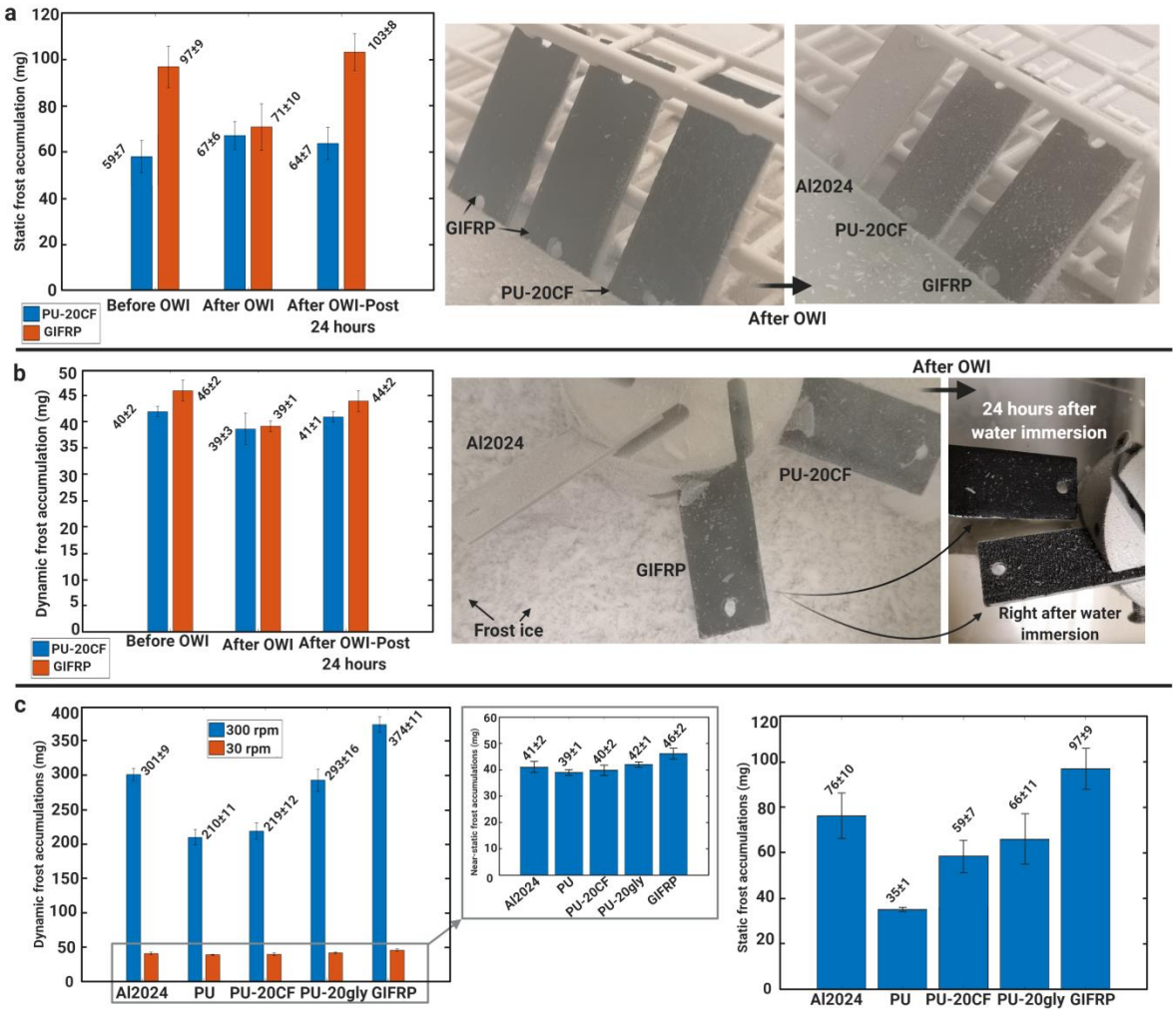

Figure 3: The accumulative data on static frost accumulation before and after 24 hours of the overnight water impression tests (experimental details are provided at the end), together with the photos of samples during the tests (a), the dynamic frost accumulation measurements at 30 rpm speeds and the relevant pictures of samples before and after the OWI tests (b), the distinctions drawn between the dynamic frost accumulations tests at two rotational speeds and a comparison is made with static frost accumulations tests (c)

Visual inspection of the glycerol-infused coatings indicated a similar observation as the static anti-icing tests and the coatings resisted the frost accumulation and accumulated condensate instead. The coatings after the dynamic tests are shown in figure 3b. The frost formation was

evident on the aluminium substrates and PU-20CF coatings, whereas negligible frost formation was observed on GIFRP coatings. Larger chunks of frost lie on the surface of GIFRP coatings and these frost chunks might have come from the frost collected by the fan in the chamber. Similar larger chunks of frost ice are also indicated on the icing plate shown in figure 3b, which might have sprinkled due to the centrifugal action of fan blades. The results, in correlation with the static anti-icing tests, suggest that skin-inspired GIFRP coatings were effective in resisting the frost formation/ice nucleation on the surfaces and were mostly kept ice-free for the duration of tests as compared to the dry polyurethane coatings and metallic substrates.

3.3.3 Effect of overnight water immersion on anti-icing properties

The initial results on GIFRP coatings suggested promising anti-icing performance, both in terms of static and dynamic anti-icing tests. The GIFRP coatings were immersed in distilled water for 24 hours and the static and dynamic anti-icing tests were repeated on the coatings. Overnight immersion of the glycerol-infused coatings in water could have an effect on the retention of glycerol in the polyurethane matrix and anti-icing performance might be hampered. Repeated test results are illustrated in figure 3a (static tests) and figure 3b (dynamic tests). The static frost accumulation tests on water-immersed PU-20CF and GIFRP coatings resulted in a similar magnitude of frost, indicating the effect of glycerol on anti-icing performance was nullified after the overnight water immersion. A similar outcome was observed on the dynamic anti-icing tests as well. The nullified anti-icing performance of water immersed GIFRP coatings as compared to that of PU-20CF coatings is shown in figure 3a. The figure indicated no difference in frost accumulations on the glycerol-infused coating as compared to the dry coatings. To ascertain the obtained results, the anti-icing tests were again repeated after 24 hours of initial overnight water immersion. The anti-icing performance of GIFRP coatings was restored and the coatings again

started to resist the frost accumulation. The 24-hours post-water immersion surface of GIFRP is shown in figure 3b. These tests suggest that the GIFRP coatings may possess the capability to self-heal or the coatings could release the infused liquid slowly to maintain icephobic performance. In either case, the coatings regained the icephobic performance after 24 hours of the overnight water immersion tests. It is imperative to mention that both tests were conducted at the intervals of 24 hours each and durability studies with time can be studied in the future.

3.3.4 Impact of erosion on de-icing properties

Ice adhesion strength tests were conducted on all the studied polyurethane coatings and as-received aluminium substrates. The centrifugal method to evaluate the ice adhesion strength in this work had been previously applied by many researchers[32-34], and a recent comparative study indicated its compatibility with the other widely used methods such as the horizontal force transducer method[35]. However, on bulk ice formations, a systematically higher shear strength was observed on the push methods as compared with that of the centrifugal methods. The ice adhesion results before and after WIETs are summarised in figure 2b. The ice adhesion on the aluminium substrates was ~145 kPa and ~2.6 kPa on pure PU coatings, a ~56-fold reduction in ice adhesion on pure PU surfaces. The incorporation of 20 wt% carbon fibres in the polyurethane matrix increased the ice adhesion by ~2 fold to 5.8 kPa as compared to that of pure PU coatings. The infusion of glycerol in pure PU and PU fibre-reinforced coatings resulted in ice adhesion of 0.15 kPa and 0.32 kPa, respectively. Pure PU coatings exacerbated the ice adhesion after the erosion tests to 83.1 kPa, a ~32 fold increase. Similarly, ice adhesion on PU-20gly coatings increased by ~37 fold after the erosion tests. These steep increase in ice adhesions may suggest a greater number of possible ice anchoring points (surface cavities) generated by the impinging particles as indicated from the increase of the surface roughness of the samples.

The incorporation of carbon fibres was successful in restricting the morphological damages caused by the impacting droplets/sand particles on the surfaces, which could be supported by figure S2. The ice adhesion of PU-20CF coatings increased by a mere ~1.5 fold after the erosion tests, as compared to a ~32-fold increase on pure PU coatings. The impinged PU-20gly coatings indicated a higher change in surface roughness as compared to that of PU and PU-20CF coatings, however, resulted in a lower ice adhesion. This reduction on PU-20gly coatings gives the idea that glycerol was still suppressing a stronger interaction between the ice and the surface even after the erosion tests. The results obtained on GIFRP coatings were most promising and the ice adhesion increased from 0.22 kPa to 0.77 kPa after the erosion tests. These values are one of the lowest ice adhesion strengths reported in the literature after the coatings have been damaged and table S2 is provided in the supplementary information to compare the ice adhesion strength and durability evaluation of the recent icephobic coatings from literature. A surface is believed to be icephobic if the ice adhesion is maintained below 10 kPa and ice adhesion on the hybrid GIFRP coatings was kept below 1 kPa after the erosion tests.

3.4 Durability enhancement and liquid retention mechanisms

The impinging droplets/sand particles create multiple stress waves on the impact zone and these stress waves consist of three multidirectional waves[36]. These stress waves are detrimental to the durability of coatings and may impart structural abnormalities, especially on the surface, if the stress waves exceed the dynamic fracture strength of the target material[37]. The effect of these waves are often connected with the fatigue properties as the material experience repetitive loads and the fractures caused by the erosion may lead to a fatigue failure[38]. However, Alder et al.[39] indicated that fatigue plays a secondary role, and concluded that the topological changes (microstructural discontinuities) or stress concentrations on the cracks during the incubation

period are the main factors that accelerate the erosion rate. Thus, minimising the surface damage is the key to achieving the lasting icephobic performance, as it will mitigate the erosion rate, as well as provide a minimal number of possible ice anchoring points[40]. In this paper, the impingement test consists of a mixture of water with hard SiC particles, and the particles could inflict more damage as compared to that of water droplets. The results conducted in this work indicate that the crack initiations to be a lead factor as the reinforced fibre composites demonstrated fewer surface anomalies after the erosion tests. The incorporation of fibres in the matrices results in better loading transfer and the increase of coating toughness. Thus, the capability of composite to withstand repetitive impact loads is greatly enhanced.

Additionally, high erosion resistance on elastomers, like the one used in this paper, is linked to their viscoelastic behaviour and low modulus enables elastomers to dissipate the impact energy and prevents the pressure buildup, thus avoiding the stress concentrations across the surface[41]. Likewise, a low modulus elastomer could also provide a path for easy release of ice (low ice adhesion) due to a mismatch in strain under stress and large moduli difference between soft and ice surfaces[18-19]. On the other hand, the fibre structure in the polyurethane matrix could effectively withstand the impacting energy by distributing the kinetic energy of water droplet/sand particles across the discontinuous fibre structure without causing any significant damage. In the structure of the skin, the response of the discontinuous collagen fibrils to an external loading could effectively prompt stress redistribution and prevent the stress concentration in one area, leading to substantial energy dissipation[23]. The fibre-reinforced coatings studied in this paper were incorporated with milled carbon fibres, instead of typical long fibres to produce an isotropic response to the impacting particles and also providing a discontinuous path for impacting energies. However, the introduction of milled carbon fibres

came with a trade-off of using a lower aspect ratio (length/depth) of the fibres and higher aspect ratios are indicated to have greater fatigue resistance[42]. Generally, the erosion process on fibre-reinforced elastomeric composite seems to take place in two modes[25]. Firstly, the local resin removal results in exposure of fibres to the erosive environment, as shown in the 3D profile in figure 1c. Secondly, a possible breakage of fibres as a result of direct impingement (as a result of plastic deformation) and the cracks start to form around the fibre interface.

Another important aspect is the liquid retention in the polyurethane matrix. Most of the slippery or liquid infused coatings are faced with existential problems such as poor durability and the depletion of infused liquid over time or due to material damage. With each frosting/defrosting cycle, a portion of the lubricant was lost either via wicking away or evaporation[43-46].

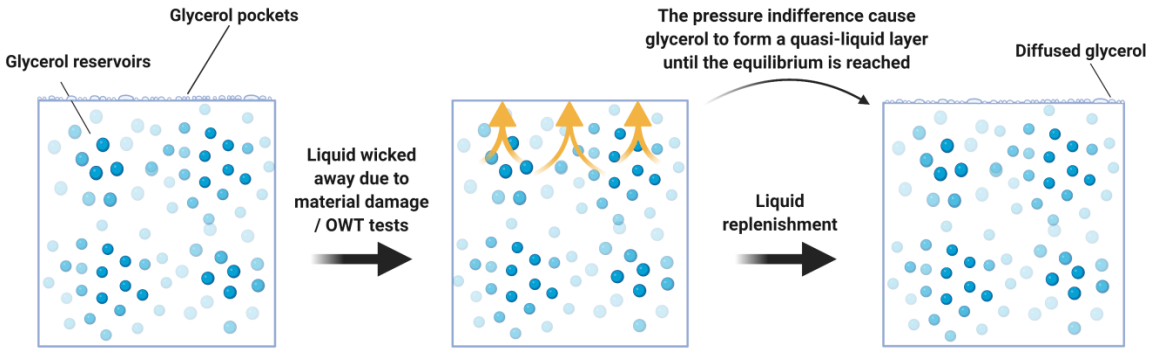

Figure 4: Liquid replenishment process on GIFRP coatings via diffusion after the glycerol pockets were wicked away (created using Biorender.com)

The infused glycerol in the polyurethane matrix could be supplemented through the diffusion on the surface, like the cetacean skin type lipid droplets emit oil to improve hydrodynamics, mainly due to capillary wick action, where the fluidic nature of the infused liquid spontaneously refills the physical voids[47]. The inclusion of glycerol could also be used to resemble the lipid droplets in a cetacean skin type, providing a flexible liquid-like interface that may act as a squeezable

temporary refuge to store the elastic potential energy until the load is transferred to the collagen fibres and/or the tissues to dissipate the energy[48]. The glycerol forms a quasi-liquid layer on the surface and when the surfaces are impacted using the erosion technique or the glycerol is wicked away, the coating squeezes glycerol on the surface via capillary wicking to maintain a quasi-liquid layer until equilibrium is reached as shown in figure 4. The diffusion of glycerol may not be affected by the erosion damage as the glycerol reservoirs are uniformly distributed across the coating matrix. The long-term stability and resilience of infused liquid coatings are further associated with low viscosity liquids and using a working liquid with different surface tension than that of interacting liquids[47, 49]. Glycerol satisfies both conditions and the viscosity is likely to decrease with sub-zero temperatures[50]. However, the studies concerning the stability of infused liquids are limited to fluorinated, silicon, and minerals oils[47, 51]. Sun et al.[2] conducted a similar study, like the one debated in this paper, using propylene glycol and reported promising stability of the infused liquid over a variety of anti-icing analyses. The design of GIRRP coatings enables the effective retention of the infused liquid within the fibrous structure. This strategy offers an alternative promising design as compared to other liquid-infused surfaces, which use either porous or textured impregnated surfaces to ensure the stability of the infused liquid, rather than reinforcing the matrix materials. It is imperative to mention that some degree of dissolution is inevitable as glycerol is highly miscible with water, however, the solubility of glycerol could be considered in other beneficial factors. Firstly, the solubility of glycerol during the crystallisation process creates a misfit between the water molecules, which results in ice not being strongly adhered to the polyurethane surface. The presence of glycerol in the water droplets also works to disrupt the ice crystal lattice formation by forming stronger hydrogen bonds with water molecules and competing against the water-water hydrogen bonding[30], which

could be the case for the anti-icing results, when mainly the condensate was accumulated on the surface (resisting frosting) and the surface was majorly frost-free. Secondly, the glycerol-water miscibility was investigated at a range of salinities and temperature levels[52], which offers a promising potential of icephobic performance for offshore and aerospace applications. Additionally, the infusion of glycerol also does not pose any environmental challenges as the infused liquid is a natural alcohol and is not as toxic as many fluorinated infusions studied in the literature[53-55].

The synergetic effect of ice depression induced by the infusion of glycerol and structural strength properties and crack inhibition capabilities provided by the incorporation of carbon fibres in the polyurethane matrix imparted continued icephobic performance after the erosion impacts. A layer of infused glycerol (in form of liquid pockets) was present on the surface even after the severe erosion damages and the incorporation of fibres could be the reason behind the retention of infused liquid in the polyurethane matrix.

4 Conclusions

The development of erosion-resistant glycerol-infused fibre-reinforced polyurethane (GIFRP) coatings was carried out by mimicking the surface structure of the cetacean skin. On the other hand, the supercooling point was reduced with the infusion of glycerol, inspired by chionophiles such as wood frogs and red flat dark beetles. The main aspirations behind the coating design were to address the performance challenges of liquid-infused icephobic coatings, such as coating durability, the depletion of infused or impregnated liquid, and the inability to maintain a smoother morphology after material/surface damage.

An effective and sustained presence of glycerol was instrumental to the surface being virtually ice/frost-free for the duration of static and dynamic anti-icing tests. The infusion of glycerol assisted by delaying water droplet freezing time to ~364-372 seconds, a 659% increase in freezing delays as compared to that of aluminium substrates. At the same time, the adaptation of the fibrous structure in the coatings helped in two distinctive ways. Firstly, the fibre network was efficient in retaining the infused liquid inside the polyurethane matrix after surface damages and the replenishment was possible due to the diffusion of infused liquid. Secondly, the restriction of surface damage caused the ice adhesion to reduce to 0.77 kPa on the GIFRP coatings, as compared to that of 83.1 kPa on pure PU coatings after the erosion tests. Thus, the synthesised bio-inspired coatings not only reduced the ice adhesion magnitude by a ~107 fold after the erosion tests but also maintained the ice adhesion strength of less than 1 kPa.

5 Experimental details

Four types of PU coatings were formulated in this study, and each coating was characterised and compared in terms of surface roughness, morphology, and ice adhesion strength before and after the erosion test. Error bars were calculated based on a standard deviation of the measured values.

5.1 Substrates and raw materials

Aluminium 2024-T4 plates with a size of 50 mm x 20 mm x 1 mm were used as substrates. Two-part thermoset polyurethane resin namely PMC-790 (PU) was purchased from Smooth-on (USA). Carbiso Mil 100μ (milled carbon fibres, 80-100 μm average length) was obtained from Easy Composites Ltd (UK). Silicon carbide particles (SC224 600 mesh) for the water impinging erosion test were supplied from Simba Materials (UK). Triton X-100 was purchased from Sigma-Aldrich (UK).

5.2 Preparation of coatings

All aluminium plates were sandblasted to enhance the coating adhesion, using a Guyson F1200 sandblaster with 180-220 μm alumina particles. The substrates were then washed with ethanol and deionized water thrice and dried using compressed air before the coating application.

PU solutions were magnetically stirred at a Part A : Part B ratio of 2 : 1 by weight. Carbon fibres and/or glycerol were gradually introduced and mixed in the resin solution during the stirring. The PU resins were then ultrasonically mixed for a further 30 minutes, and brush coated on the sandblasted aluminium substrates. The PU (with/without the infusion of glycerol) coatings were cured at 25 ^{o}C for 48 hours and the PU coatings without glycerol infusion were followed with post-treatment at 65 ^{o}C for 4 hours. The prepared liquid-infused coatings were dry to touch.

5.3 Surface characterisation

A Zeta-20 non-contact optical profiler was used to evaluate the surface roughness. The schematic diagram of the profiler is depicted in figure S3a. The reported roughness values were the average of a minimum of 30 measurements and the standard deviation of these measurements was adapted as error limits. R_a was measured over a line stretching across the observed surface. The same system was also used to observe topographical changes after erosion. An FEI Quanta 650 ESEM (environmental scanning electron microscope) was used to acquire microstructural images and morphological damages on the eroded coatings.

Shore hardness was measured using a SAUTER durometer having Shore hardness A and D scales. The durometer was attached to SAUTER test stands TI-AO and TI-D for Shore hardness A and D scales, respectively. The hardness studied were an average penetration (Shore) value based on 10 separate measurement.

5.4 Evaluation of hydrophobicity

The sessile drop technique was used to measure water contact angles (WCAs) using an FTÅ200 goniometer and 5 µl of a controlled volume of water drop was analysed. The schematic diagram of the goniometer is shown in figure S3b. The tests were conducted at room temperature.

5.5 Ice adhesion strength tests

A MOOG G403-2053A servo motor was used to measure the ice adhesion strength tests via a centrifugal method and the test was performed in an environmental chamber (ALPHA 1550-40H) to simulate the freezing conditions. The ice adhesion test was conducted at a temperature of -10 ^{o}C.

The ice adhesion force F (N) is determined using,

$$F = mr\omega^2 \quad (1)$$

Where ω (rad/s) is the rotational speed at the point of ice removal, r (m) is the rotor length, and m (kg) is the mass of ice. The ice (shear) adhesion strength τ_{ice} can then be calculated as,

$$\tau_{ice} = {}^{F}/_{A} \quad (2)$$

Where A (m^2) is the substrate/ice contact area.

The static and dynamic water contact angles (WCAs), including advancing WCAs (AWCAs), receding WCAs (RWCAs), contact angle hysteresis (CAH), and ice adhesion strength measurements are summarized in table S1.

5.6 Anti-icing tests

All the anti-icing tests were conducted in a custom-built chamber located on RZ Medizintechnik GmbH Peltier cooling plate. The temperature around the testing area was monitored using an

open K-type thermocouple which was placed near the samples during the tests. In all the tests, a fan, circulating the airflow at ~3.8 m/s (or ~32 CFM), was operational to ensure temperature consistency in the chamber.

5.6.1 Water droplet freezing delay test

The ambient temperature was set at -11 ^{o}C for water droplet freezing delays tests. The surface temperature was monitored using a high-temperature type K surface probe and maintained at -10 ^{o}C. The figure depicting the system is shown in figure S4. A controlled volume, 5 µl, was dispensed using a syringe pump on ten different spots of the samples and an average of the freezing delays was calculated.

5.6.2 Static anti-icing tests

The samples were placed at 45^{o} angle against a metal stand and facing nebulised water aerosols. The nebulised water aerosols were generated using Omron Ultrasonic Nebulizer NE-U17. A total of 20 ± 2 ml of aerosol was fed into the system to encourage condensation/frosting and simulate stormy icing conditions. The nebulised water aerosols were maintained throughout the tests and the volume was monitored. The schematic diagram of the system is shown in figure 5. The ambient temperature of around -14 ^{o}C was maintained throughout the tests (measured through an open K-type thermocouple) and the surface temperature (of Peltier cooling plate) was set at -15 ^{o}C. The test duration was one hour and the weight of frost accumulated was measured. Each test was repeated three times and an average was calculated. The surface was pictured via a high definition camera thrice during the ice accumulation process to understand the ice nucleation over the different surfaces.

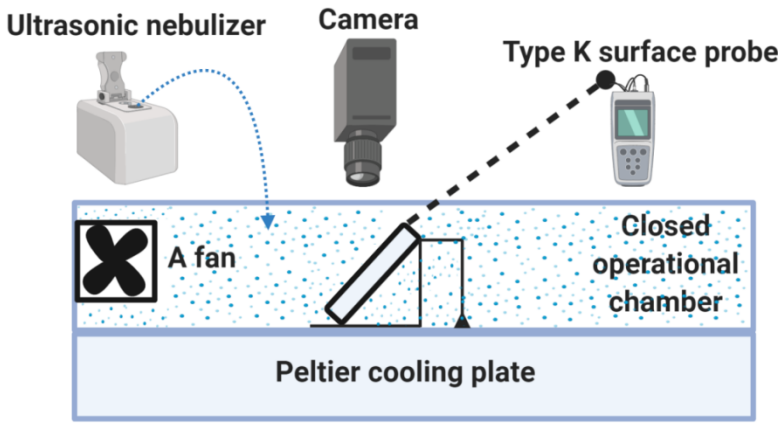

Figure 5: A depiction of static anti-icing test setup (created using biorender.com)

5.6.3 Rotary dynamic anti-icing tests

A custom-built metal rotor with 6 seats for samples was used for rotary tests. The samples were fastened by means of a screw and the rotor was spun at 30 rpm in similar humid conditions as static anti-icing tests. The system is visualised in figure 6. To ensure repeatability and to expose the coated surface only, the backside or metallic side of the samples were covered by peel-able tape and the tape was peeled after the tests. The ice accumulation was measured after an hour of test and an average of three tests was calculated. The samples were also pictured after the tests and a sample test is visualized in video S1.

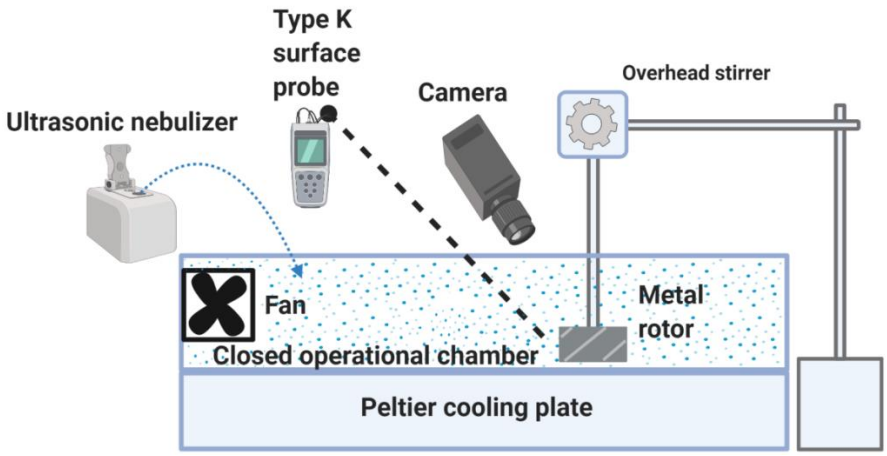

Figure 6: A depiction of rotary dynamic anti-icing test setup (created using biorender.com)

5.6.4 Anti-icing test after an overnight water immersion

The technique was deployed to understand the retention and influence of glycerol on anti-icing performance. The technique involved submerging the samples in distilled water for 24 hours and the static and dynamic anti-icing tests were repeated on GIFRP coatings. Furthermore, anti-icing tests were again repeated on water-immersed coatings after 24 hours of first testing to ascertain the obtained results. In total, there were two tests conducted in 48 hours. The tests were carried along PU-20CF coatings to compare the GIFRP coatings in similar environments and conditions.

5.7 Water impinging erosion tests (WIETs)

To evaluate the coating durability, a silicon carbide suspension based erosion test was carried out. The silicon carbide suspension was prepared using 1 wt% silicon carbide microparticles and was suspended using 0.1 wt% of Triton X-100. The suspension was magnetically stirred for 4 hours. During the test, the suspension was pressurized through a PNR ultrasonic atomiser nozzle (MAD 0331 B1BB) using compressed gas and the micro-droplets impinged onto the coated specimen. The schematic diagram of the impingement system is shown in figure 7. The system was kept and maintained at a liquid flow rate of 1.2 mL/s, the distance between the nozzle and a specimen of 4 cm and a duration of 90 min. The surface morphology, surface roughness, and ice adhesion strength of the coatings were measured before and after the erosion tests.

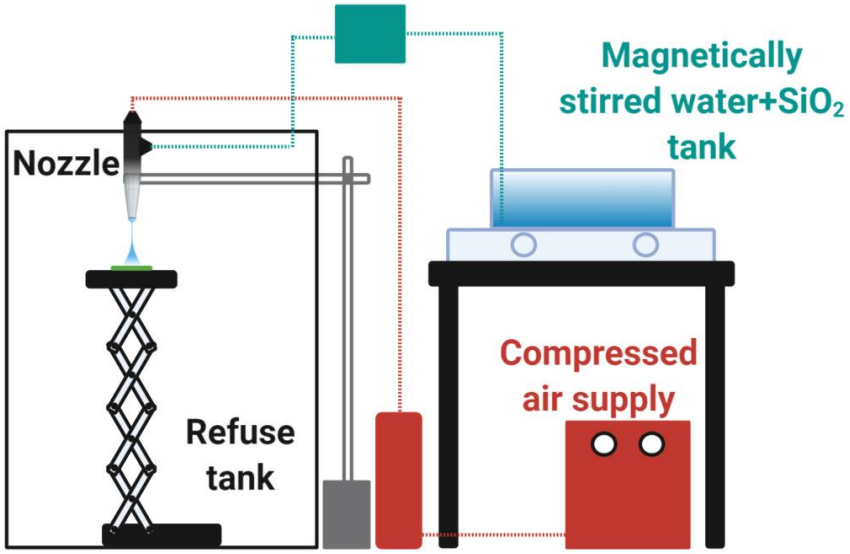

Figure 7: A depiction of water impinging erosion test setup (created using biorender.com)

Declaration of Competing Interests

There are no conflicts to declare.

Supporting Information

- Microstructural image of the aluminium sample, microstructural images and 3D profiles of the PU coatings before and after the erosion tests, schematic diagrams of the surface profiler, goniometer, and water droplet icing delay test setup (Figures S1-S4).
- Complete list of the performance evaluation data of the studied samples/coatings and a comparison of ice adhesion strengths and durability of the recent icephobic coatings (Tables S1 and S2).
- Visual demonstration of dynamic anti-icing test setup (Movie S1).

Author Contributions

Halar Memon: Conceptualisation, Methodology, Software, Validation, Investigation, Formal analysis, Writing-Original draft, and Visualisation.

Davide S.A. De Focatiis: Conceptualisation, Resources, Writing-Review and Editing, and Supervision.

Kwing-So Choi: Conceptualisation, Project administration, Funding acquisition, Writing-Review and Editing, and Supervision.

Xianghui Hou: Conceptualisation, Project administration, Resources, Data Curation, Funding acquisition, Writing-Review and Editing, methodology, and Supervision.

Acknowledgements

This work was supported by a studentship from the Faculty of Engineering, University of Nottingham and was partially funded by the CleanSky 2 Joint Undertaking under the European Union's Horizon 2020 research and innovation programme under grant agreement No CS2-AIR-GAM-2014-2015-O1. Cf. Art.29.4 of [A2]. The authors also thank Dr. Barbara Turnbull for helping with ice adhesion strength tests and acknowledge the use of facilities at the Nanoscale and Microscale Research Centre of the University of Nottingham supported by Engineering and Physical Sciences Research Council [grant number EP/L022494/1].

References

(1) Liu, F.; Pan, Q. Facile Fabrication of Robust Ice-Phobic Polyurethane Sponges. Adv. Mater. Interfaces 2015, 2 (15), 1500219, DOI: 10.1002/admi.201500219.

(2) Sun, X.; Damle, V. G.; Liu, S.; Rykaczewski, K. Bioinspired Stimuli-Responsive and Antifreeze-Secreting Anti-Icing Coatings. Adv. Mater. Interfaces 2015, 2 (5), 1400479, DOI: 10.1002/admi.201400479.

(3) Charpentier, T. V. J.; Neville, A.; Millner, P.; Hewson, R.; Morina, A. An Investigation of Freezing of Supercooled Water on Anti-Freeze Protein Modified Surfaces. J Bionic Eng 2013, 10 (2), 139-147, DOI: 10.1016/S1672-6529(13)60208-5.

(4) Gwak, Y.; Park, J.-i.; Kim, M.; Kim, H. S.; Kwon, M. J.; Oh, S. J.; Kim, Y.-P.; Jin, E. Creating Anti-icing Surfaces via the Direct Immobilization of Antifreeze Proteins on Aluminum. Sci Rep 2015, 5 (1), 12019, DOI: 10.1038/srep12019.

(5) Kasahara, K.; Waku, T.; Wilson, P. W.; Tonooka, T.; Hagiwara, Y. The Inhibition of Icing and Frosting on Glass Surfaces by the Coating of Polyethylene Glycol and Polypeptide Mimicking Antifreeze Protein. Biomolecules 2020, 10 (2), 259, DOI: 10.3390/biom10020259.

(6) Koshio, K.; Waku, T.; Hagiwara, Y. Ice-phobic glass-substrate surfaces coated with polypeptides inspired by antifreeze protein. Int. J. Refrig. 2020, DOI: 10.1016/j.ijrefrig.2020.01.025.

(7) Vazirinasab, E.; Maghsoudi, K.; Jafari, R.; Momen, G. A comparative study of the icephobic and self-cleaning properties of Teflon materials having different surface morphologies. J. Mater. Process. Technol. 2020, 276, 116415. DOI: 10.1016/j.jmatprotec.2019.116415.

(8) Piscitelli, F.; Chiariello, A.; Dabkowski, D.; Corraro, G.; Marra, F.; Palma, L. D. Superhydrophobic Coatings as Anti-Icing Systems for Small Aircraft. Aerospace 2020, 7 (1), 2, DOI: 10.3390/aerospace7010002.

(9) Wu, X.; Silberschmidt, V. V.; Hu, Z.-T.; Chen, Z. When superhydrophobic coatings are icephobic: Role of surface topology. Surf. Coat. Technol. 2019, 358, 207-214, DOI: 10.1016/j.surfcoat.2018.11.039.

(10) Tas, M.; Memon, H.; Xu, F.; Ahmed, I.; Hou, X. Electrospun nanofibre membrane based transparent slippery liquid-infused porous surfaces with icephobic properties. Colloids Surf. A Physicochem. Eng. Asp. 2020, 585, 124177, DOI: 10.1016/j.colsurfa.2019.124177.

(11) Cui, W.; Pakkanen, T. A. Icephobic performance of one-step silicone-oil-infused slippery coatings: Effects of surface energy, oil and nanoparticle contents. J. Colloid Interf. Sci. 2020, 558, 251-258, DOI: 10.1016/j.jcis.2019.09.119.

(12) Tetteh, E.; Loth, E. Reducing Static and Impact Ice Adhesion with a Self-Lubricating Icephobic Coating (SLIC). Coatings 2020, 10 (3), 262, DOI: 10.3390/coatings10030262.

(13) Memon, H.; Liu, J.; Weston, N.; Wang, J.; De Focatiis, D.; Choi, K.-s.; Hou, X. In-situ icing and water condensation study on different topographical surfaces. Cold Reg. Sci. Technol. 2019, 102814, DOI: 10.1016/j.coldregions.2019.102814.

(14) Memon, H.; Liu, J.; De Focatiis, D. S.; Choi, K.-s.; Hou, X. Intrinsic dependence of ice adhesion strength on surface roughness. Surf. Coat. Technol. 2020, 385, 125382, DOI: 10.1016/j.surfcoat.2020.125382.

(15) Zhou, C.; Zhao, X.; Zhao, X.; Li, H.; Zhang, S.; Feng, W.; Zhang, Y. Low Ice Adhesion Surfaces Based on Flexible Fluorinated Polymers with a Polynorbornene Backbone. ACS Appl. Mater. Interfaces 2020, 12 (47), 53494-53502, DOI: 10.1021/acsami.0c15627.

(16) Li, T.; Ibáñez-Ibáñez, P. F.; Håkonsen, V.; Wu, J.; Xu, K.; Zhuo, Y.; Luo, S.; He, J.; Zhang, Z. Self-Deicing Electrolyte Hydrogel Surfaces with Pa-level Ice Adhesion and Durable Antifreezing/Antifrost Performance. ACS Appl. Mater. Interfaces 2020, 12 (31), 35572-35578, DOI: 10.1021/acsami.0c06912.

(17) Gao, J.; Martin, A.; Yatvin, J.; White, E.; Locklin, J. Permanently grafted icephobic nanocomposites with high abrasion resistance. J. Mater. Chem. A 2016, 4 (30), 11719-11728, DOI: 10.1039/C6TA03222B.

(18) Golovin, K.; Kobaku, S. P. R.; Lee, D. H.; DiLoreto, E. T.; Mabry, J. M.; Tuteja, A. Designing durable icephobic surfaces. Sci. Adv. 2016, 2 (3), e1501496, DOI: 10.1126/sciadv.1501496.

(19) Wang, C.; Fuller, T.; Zhang, W.; Wynne, K. J. Thickness dependence of ice removal stress for a polydimethylsiloxane nanocomposite: Sylgard 184. Langmuir 2014, 30 (43), 12819-12826, DOI: 10.1021/la5030444.

(20) Ling, J. K. The integument of marine mammals. Functional anatomy of marine mammals 1974, 2, 1-44.

(21) Reeb, D.; Best, P. B.; Kidson, S. H. Structure of the integument of southern right whales, Eubalaena australis. The Anatomical Record 2007, 290 (6), 596-613, DOI: 10.1002/ar.20535.

(22) Mouton, M.; Botha, A. Cutaneous lesions in cetaceans: an indicator of ecosystem status, InTech: 2012.

(23) Yang, W.; Sherman, V. R.; Gludovatz, B.; Schaible, E.; Stewart, P.; Ritchie, R. O.; Meyers, M. A. On the tear resistance of skin. Nat. Commun. 2015, 6 (1), 6649, DOI: 10.1038/ncomms7649.

(24) Van den Berg, F. 4.3 - Extracellular matrix. In Fascia: The Tensional Network of the Human Body; Schleip, R.; Findley, T. W.; Chaitow, L.; Huijing, P. A., Eds.; Churchill Livingstone: Oxford, 2012, 165-170.

(25) Boggarapu, V.; Gujjala, R.; Ojha, S. A critical review on erosion wear characteristics of polymer matrix composites. Materials Res. Express 2020, 7 (2), 022002, DOI: 10.1088/2053-1591/ab6e7b.

(26) Pfeiffer, C. J.; Jones, F. M. Epidermal lipid in several cetacean species: ultrastructural observations. Anat. Embryol. 1993, 188 (3), 209-218, DOI: 10.1007/BF00188213.

(27) Trejo González, J. A.; Longinotti, M. P.; Corti, H. R. The Viscosity of Glycerol−Water Mixtures Including the Supercooled Region. J. Chem. Eng. Data 2011, 56 (4), 1397-1406, DOI: 10.1021/je101164q.

(28) Storey, K. B.; Storey, J. M. Biochemistry of Cryoprotectants. Insects at Low Temperature, Springer US: Boston, MA, 1991, 64-93.

(29) Carrasco, M. A.; Buechler, S. A.; Arnold, R. J.; Sformo, T.; Barnes, B. M.; Duman, J. G. Investigating the deep supercooling ability of an Alaskan beetle, Cucujus clavipes puniceus, via high throughput proteomics. J. Proteom 2012, 75 (4), 1220-1234, DOI: 10.1016/j.jprot.2011.10.034.

(30) Chen, C.; Li, W. Z.; Song, Y. C.; Yang, J. Hydrogen bonding analysis of glycerol aqueous solutions: A molecular dynamics simulation study. J. Mol. Liq. 2009, 146 (1), 23-28, DOI: 10.1016/j.molliq.2009.01.009.

(31) Lane, L. B. Freezing Points of Glycerol and Its Aqueous Solutions. Ind. Eng. Chem. 1925, 17 (9), 924-924, DOI: 10.1021/ie50189a017.

(32) Janjua, Z. A.; Turnbull, B.; Choy, K.-L.; Pandis, C.; Liu, J.; Hou, X.; Choi, K.-S. Performance and durability tests of smart icephobic coatings to reduce ice adhesion. Appl. Surf. Sci. 2017, 407, 555-564, DOI: 10.1016/j.apsusc.2017.02.206.

(33) Kulinich, S.; Farzaneh, M. Ice adhesion on super-hydrophobic surfaces. Appl. Surf. Sci. 2009, 255 (18), 8153-8157, DOI: 10.1016/j.apsusc.2009.05.033.

(34) Laforte, C.; Beisswenger, A. Icephobic material centrifuge adhesion test, Proceedings of the 11th International Workshop on Atmospheric Icing of Structures, IWAIS, Montreal, QC, Canada, 2005, 12-16.

(35) Rønneberg, S.; Zhuo, Y.; Laforte, C.; He, J.; Zhang, Z. Interlaboratory study of ice adhesion using different techniques. Coatings 2019, 9 (10), 678, DOI: 10.3390/coatings9100678.

(36) Gohardani, O. Impact of erosion testing aspects on current and future flight conditions. Prog. Aerosp. Sci. 2011, 47 (4), 280-303, DOI: 10.1016/j.paerosci.2011.04.001.

(37) Brunton, J. H.; Bowden, F. P. A discussion on deformation of solids by the impact of liquids, and its relation to rain damage in aircraft and missiles, to blade erosion in steam turbines, and to cavitation erosion - High speed liquid impact. Philosophical Transactions of the Royal Society of London. Series A, Mathematical and Physical Sciences 1966, 260 (1110), 79-85, DOI: doi:10.1098/rsta.1966.0031.

(38) Mahdipoor, M.; Kirols, H.; Kevorkov, D.; Jedrzejowski, P.; Medraj, M. Influence of impact speed on water droplet erosion of TiAl compared with Ti6Al4V. Sci Rep 2015, 5, 14182, DOI: 10.1038/srep14182.

(39) Adler, W. The mechanics of liquid impact. Academic Press, Treatise on Materials Science and Technology 1979, 16, 127-183.

(40) Memon, H.; De Focatiis, D. S. A.; Choi, K.-S.; Hou, X. Durability enhancement of low ice adhesion polymeric coatings. Prog. Org. Coat 2021, 151, 106033, DOI: 10.1016/j.porgcoat.2020.106033.

(41) Elhadi Ibrahim, M.; Medraj, M. Water Droplet Erosion of Wind Turbine Blades: Mechanics, Testing, Modeling and Future Perspectives. Materials 2020, 13 (1), 157, DOI: 10.3390/ma13010157.

(42) Lavengood, R. E.; Gulbransen, L. B. The effect of aspect ratio on the fatigue life of short boron fiber reinforced composites. Polym Eng Sci. 1969, 9 (5), 365-369, DOI: 10.1002/pen.760090509.

(43) Mishchenko, L.; Hatton, B.; Bahadur, V.; Taylor, J. A.; Krupenkin, T.; Aizenberg, J. Design of Ice-free Nanostructured Surfaces Based on Repulsion of Impacting Water Droplets. ACS Nano 2010, 4 (12), 7699-7707, DOI: 10.1021/nn102557p.

(44) Wilson, P. W.; Lu, W.; Xu, H.; Kim, P.; Kreder, M. J.; Alvarenga, J.; Aizenberg, J. Inhibition of ice nucleation by slippery liquid-infused porous surfaces (SLIPS). Phys. Chem. Chem. Phys 2013, 15 (2), 581-585, DOI: 10.1039/C2CP43586A.

(45) Subramanyam, S. B.; Rykaczewski, K.; Varanasi, K. K. Ice Adhesion on Lubricant-Impregnated Textured Surfaces. Langmuir 2013, 29 (44), 13414-13418, DOI: 10.1021/la402456c.

(46) Liu, B.; Zhang, K.; Tao, C.; Zhao, Y.; Li, X.; Zhu, K.; Yuan, X. Strategies for anti-icing: low surface energy or liquid-infused? RSC Adv. 2016, 6 (74), 70251-70260, DOI: 10.1039/C6RA11383D.

(47) Villegas, M.; Zhang, Y.; Abu Jarad, N.; Soleymani, L.; Didar, T. F. Liquid-Infused Surfaces: A Review of Theory, Design, and Applications. ACS Nano 2019, 13 (8), 8517-8536, DOI: 10.1021/acsnano.9b04129.

(48) Mechanical Roles in Formation of Oriented Collagen Fibers. Tissue Eng. Part B Rev. 2020, 26 (2), 116-128, DOI: 10.1089/ten.teb.2019.0243.

(49) Weisensee, P. B.; Wang, Y.; Qian, H.; Schultz, D.; King, W. P.; Miljkovic, N. Condensate droplet size distribution on lubricant-infused surfaces. Int. J. Heat Mass Transf. 2017, 109, 187-199, DOI: 10.1016/j.ijheatmasstransfer.2017.01.119.

(50) Ferreira, A. G. M.; Egas, A. P. V.; Fonseca, I. M. A.; Costa, A. C.; Abreu, D. C.; Lobo, L. Q. The viscosity of glycerol. J. Chem. Thermodyn. 2017, 113, 162-182, DOI: 10.1016/j.jct.2017.05.042.

(51) Chen, X.; Wen, G.; Guo, Z. What are the design principles, from the choice of lubricants and structures to the preparation method, for a stable slippery lubricant-infused porous surface? Mater. Horiz. 2020, 7 (7), 1697-1726, DOI: 10.1039/D0MH00088D.

(52) Takamura, K.; Fischer, H.; Morrow, N. R. Physical properties of aqueous glycerol solutions. J. Pet. Sci. Eng. 2012, 98-99, 50-60, DOI: https://doi.org/10.1016/j.petrol.2012.09.003.

(53) Kim, P.; Wong, T.-S.; Alvarenga, J.; Kreder, M. J.; Adorno-Martinez, W. E.; Aizenberg, J. Liquid-infused nanostructured surfaces with extreme anti-ice and anti-frost performance. ACS nano 2012, 6 (8), 6569-6577, DOI: 10.1021/nn302310q.

(54) Stone, H. A. Ice-phobic surfaces that are wet. ACS nano 2012, 6 (8), 6536-6540, DOI: 10.1021/nn303372q.

(55) Liu, M.; Hou, Y.; Li, J.; Tie, L.; Guo, Z. Transparent slippery liquid-infused nanoparticulate coatings. Chem. Eng. J. 2018, 337, 462-470, DOI: 10.1016/j.cej.2017.12.118.